Bull Mater Sci (2020) 43:319
https://doi.org/10.1007/s12034-020-02289-y

Semiconductivity and superhydrophobicity in an oligo-(*p*-phenyleneethynylene) (OPE)-based luminescent MOF

SYAMANTAK ROY[1], SOHINI BHATTACHARYYA[1], ARKAMITA BANDYOPADHYAY[2], SWAPAN K PATI[2] and TAPAS KUMAR MAJI[1,*]

[1]Molecular Materials Laboratory, Chemistry and Physics of Materials Unit, School of Advanced Materials, Jawaharlal Nehru Centre for Advanced Scientific Research, Bangalore 560064, India

[2]Theoretical Science Unit, School of Advanced Materials, Jawaharlal Nehru Centre for Advanced Scientific Research, Bangalore 560064, India

*Author for correspondence (tmaji@jncasr.ac.in)

MS received 21 February 2020; accepted 11 July 2020

Abstract. An oligo-(*p*-phenyleneethynylene) (OPE)-based water repellent, luminescent and electrically conducting Mg-metal-organic framework (MOF) $\{[Mg_3(OPE\text{-}C_{18})_3(H_2O)_2]\cdot 2DMF\}_n$ (**1**) has been synthesized and structurally characterized. Ultra-high water contact angles (170°) and isotropic semiconductivity have been observed in **1** in both crystalline and thin-film states. DFT calculations support a 'through bond' mode of electrical conductance. To the best our knowledge, this report is only the second instance of a superhydrophobic and electrically conducting luminescent bulk MOF.

Keywords. Oligo-(*p*-phenyleneethynylene); superhydrophobicity; semiconductivity; luminescence; bola-amphiphile.

1. Introduction

Metal–organic frameworks (MOFs) are a crystalline class of hybrid porous polymers constructed via periodic linkages between metal nodes and organic/organometallic linkers [1–5]. Research in the field of MOFs has revolutionized gas storage and separation, catalysis and membrane-based separation of gases and liquids [6–8]. MOFs have shown other promising applications as well, such as drug delivery, proton conduction, sensing and nanoscale morphology tunability [9–12]. The recent function of MOFs which is being explored is their electrical properties [13–15]. A vast choice of organic linkers with a known band structure can help to create a family of MOFs having different band gaps suited to different electrical functions [16–19]. The metal ion in MOFs also plays a significant role in controlling the coordination environment and providing the conducting pathway through its unfilled orbitals [13]. Electrical conductance in MOFs can occur in three charge transport pathways: (1) 'through space' (π-stacking), (2) 'through bond' (via covalent bonds) and (3) charge hopping, directed by the Marcus theory. All three mechanisms can be utilized to generate electrically conducting MOFs. Electrically conducting MOFs therefore, have the potential to substantially impact the energy landscape by introducing a new class of materials suitable for electrical device fabrication in Schottky barrier diodes (SBDs) [20,21], field-effect transistors (FETs) [22,23], and light-emitting diodes (LEDs) [24,25]. Coupled with water-repellence, MOFs also have the potential to be used as underwater semi-conductor devices. Structural tunability of MOFs can also induce moisture resistance via use of water repellent organic linkers for its construction [26,27].

Use of bola-amphiphilic ligands with an end-capping polar coordinating groups with an inner non-polar π-rich groups could serve the purpose of both 'through space' and 'through bond' charge transport mechanisms via its stacking interactions of the phenyl rings and assembling with metal ions through end groups, respectively. Oligo-*p*-(phenyleneethynylenes) (OPEs) are one such class of π-conjugated ligands whose synthetic tunability allows incorporation of water-repellent functional groups in the side chains and coordinating functional groups along with charge transport properties for MOF construction [28–33]. We have recently reported one such work in which the use of water repellent and electrically conducting organic linker for nanoscale MOF (NMOF) construction has led to a photo-conducting and moisture-resistant Schottky barrier NMOF diode [20].

This article is part of the Topical Collection: SAMat Focus Issue.

Electronic supplementary material: The online version of this article (https://doi.org/10.1007/s12034-020-02289-y) contains supplementary material, which is available to authorized users.

Published online: 14 December 2020

Therefore, this work along with another previous report, gives the idea that using bola-amphiphilic, π-conjugated organic linkers generate high-charge carrier mobility and also mimics the lotus leaf surface, thereby assisting in water repellence [28–33]. Taking a cue from these works, we decided to translate the same properties into bulk MOFs. Till date, only a handful of reports give an organizational understanding of surface water repellence and conducting pathways in MOFs and this would provide the advantage of a structural understanding of both the properties [34–38].

This work describes the synthesis of a bola-amphiphilic oxy-octadecyl functionalized oligo-(*p*-phenyleneethynylene) ligand (**H_2OPE-C_{18}**) for the construction of bulk MOF structures and its self-assembly with $Mg(NO_3)_2$ to get MOF single crystals $\{[Mg_3(OPE\text{-}C_{18})_3(H_2O)_2]\cdot 2DMF\}_n$ (**1**) having a 3D structure. **1** showed superhydrophobic property with an ultra-high contact angle of 170°. It also showed cyan luminescence with a high quantum yield. Electrical conductivity measurements on different faces of the single crystal and thin films showed charge transport in the semiconducting regime. **1** is therefore, a member of a small group of MOF structures showing appreciable conductivity and is also the second report of a water repellent and semiconducting MOF structure.

2. Experimental

2.1 *Materials*

$Pd(PPh_3)_4$ and $Mg(NO_3)_2\cdot 6H_2O$ were obtained from Sigma-Aldrich Chemical Co. and cuprous iodide was acquired from Loba Chemie Pvt. Ltd. N,N-dimethyl formamide (DMF) and tetrahydrofuran (THF) were obtained from Spectrochem Pvt. Ltd. (Mumbai, India). THF was pre-dried using standard procedure and all other reagents, solvents were of reagent grade and used without further purification.

2.2 *Physical measurements*

Elemental analyses were carried out using a Thermo Scientific Flash 2000 CHN analyser. Infrared spectral studies were performed by making samples with KBr pellets using Bruker FTIR spectrometer. Powder X-ray diffraction (PXRD) studies were recorded on a Bruker D8 discover instrument using CuKα radiation. Thermal stability was analysed using Mettler Toledo TGA 800 instrument under inert atmosphere in the temperature range of 25–850°C at a heating rate of 3°C min^{-1}. UV–Vis spectra were recorded on a Perkin Elmer Model Lambda 900 spectrophotometer. Fluorescence studies were accomplished using Perkin Elmer Ls 55 luminescence spectrometer. Fluorescence lifetime measurements were recorded with a Horiba Deltaflex spectrometer. Electrochemical performance of **1** was measured by using a glassy carbon electrode (GCE) voltammetry. They were performed using an Autolab PGSTAT12 potentiostat/galvanostat in a conventional three-electrode cell.

2.3 *Adsorption measurements*

Porosity measurements of **1** were carried out using QUNATACHROME QUADRASORD-SI analyser at 77 K for N_2 and 195 K for CO_2. In the sample tube, the adsorbent samples (∼100–150 mg) were placed which have been prepared at 170°C under a 1×10^{-1} Pa vacuum for about 12 h prior to measurement of the isotherms. Helium gas (99.999% purity) at a certain pressure was introduced in the gas chamber and allowed to diffuse into the sample chamber by opening the valve. The amount of gas adsorbed was calculated from the pressure difference (P_{cal}–P_e), where P_{cal} is the calculated pressure with no gas adsorption and P_e is the observed equilibrium pressure. All the operations were computer-controlled. Benzene and water vapour adsorptions were carried out at 298 K using BELSORP AQUA 3 solvent vapour analyser. A sample of about ∼100–150 mg was prepared by heating at 170°C for about 12 h under vacuum (1×10^{-1} Pa) prior to measurement of the isotherms. The solvent molecules used to generate the vapour were degassed fully by repeated evacuation. Dead volume was measured with helium gas. The adsorbate was placed into the sample tube, then the change of the pressure was monitored and the degree of adsorption was determined by the decrease in pressure at the equilibrium state. All operations were computer-controlled and automatic.

2.4 *Conductivity measurements*

Conductivity measurement on a thin film of the material was performed on a glass substrate by spin coating technique at 1200 rpm for 2 min and subsequently dried. Two ohmic parallel electrodes were taken from the film. The dimensions of the electrodes were of 9×1 mm^2 with a gap of 1 mm between two electrodes. For conductivity measurement, a two-probe contact method was adopted to obtain a current–voltage (*I–V*) characteristics graph, where the electrodes were connected with a Keithley 2450 sourcemeter. The process was performed under room temperature and in an open atmosphere. The conductivity was measured with the help of the slope of linear fitted *I–V* curve, by using the equation:

$$\sigma = \left(\frac{\Delta I}{\Delta V}\right)\left(\frac{l}{A}\right),$$

where σ is the conductivity, I the current, V the applied voltage, l the distance between electrodes and A the cross-sectional area of the sample.

The same equation was used to measure conductivities on single crystals of **1**. Silver paste contacts were made on

different faces of single crystals of **1**. Copper wires were attached to the silver paste contacts and *I–V* profiles were measured using a Keithley 2450 sourcemeter under open atmosphere.

3. Results and discussion

H_2OPE-C_{18} was synthesized according to reported Sonogashira–Hagihara coupling procedures (supplementary scheme S1). Block-shaped green crystals of **1** were obtained after 10 days by layering an ethanolic solution of $Mg(NO_3)_2$ onto a buffer layer on a DMF solution of **H_2OPE-C_{18}** in a 1:1 molar ratio. Single crystal XRD (SCXRD) analysis revealed that **1** crystallizes in a triclinic crystal system with a $P\bar{1}$ space group (supplementary table S1, CCDC no. 1975641). The structure of **1** having the formula of $Mg_3(O_2C)_6(OH_2)_2$ can be visualized as an extension of a Mg_3-core secondary building unit (SBU) via OPE dicarboxylate linkages in two crystallographic axes (figure 1a). There are two crystallographically independent Mg^{II} atoms, Mg1 and Mg2 in the structure. Each Mg1 is penta-coordinated and connected to four carboxylate oxygen atoms (O1, O4, O7 and O8) from three different OPE-C_{18}. The fifth position is occupied by a water molecule (O10). Each Mg2 is hexa-coordinated and connected to six carboxylate oxygen atoms (O2, O3, O7 and its symmetry related counterparts). One OPE-C_{18} (OPE-C_{18})$_1$ dicarboxylate connects four Mg^{II} centres by *syn–syn* bridging (O1, O2 and O3, O4) and acts as a tetradentate ligand, whereas the other OPE-C_{18} (OPE-C_{18})$_2$ binds to four Mg^{II} centres by μ-oxo bridging (μ_2-O1) as well as cis-chelating (O7, O8) (figure 1a). Two symmetry related (OPE-C_{18})$_1$ binds the further connected by (OPE-C_{18})$_2$ to form a 2D grid-like porous structure in the *bc* plane (supplementary figure S2, figure 1b, c). There are very weak C−H$^{\cdots}$π interactions between the alkyl chains and π-cores of adjacent OPEs building the column. This further reinforces the 1D packing in **1**. Another interesting feature of the structure of **1** is that there are long oxyoctadecyl chains decorated towards the periphery of the porous structure (figure 1d). The Mg–O bond distances are in between 1.857(15)–2.259(17) Å (supplementary table S2), which comfortably falls within the expected Mg–O bond distances with no anomaly.

Presence of water molecules in **1** was further confirmed from the infrared (IR) spectrum (supplementary figure S3). TGA analysis of the as-synthesized **1** shows a weight loss of 3% between 160–180°C following which the structure was stable up to 300°C (supplementary figure S4). The mass loss of 3% corresponds to the loss of guest DMF molecules. Porosity measurements were carried out after degassing **1** at 180°C overnight. **1** was non-porous towards N_2 as deduced from the type II isotherm at 77 K (supplementary figure S5). However, it showed a gradual uptake of 50 cc g^{-1} CO_2 at 195 K up to a pressure of 1 bar (figure 2a). This adsorption behaviour can be attributed to protruding octadecyl side chains limiting pore size of **1**. CO_2 having a smaller kinetic diameter (3.30 Å) than N_2 (3.64 Å) can easily diffuse into the pores of **1** leading to a selective uptake of CO_2 over N_2 for this framework. PXRD analysis indicated a high degree of crystallinity in **1** which was maintained in the degassed sample as well (supplementary figures S6 and S7). The high degree of crystallinity, porosity, conjugation and long alkyl chains present in the structure further motivated us to investigate its luminescent, charge transport and water repellent properties.

It has been well studied that surface-projected alkyl and fluoroalkyl chains increase the surface roughness, decrease the surface energy and thereby induce superhydrophobicity in a structure [26,27,31]. As our ligand also contained long alkyl chains, we decided to check for its water repellence property first. Water contact angles measured on a glass substrate coated with **H_2OPE-C_{18}** showed a contact angle of 140–145° as was previously reported by us (supplementary figure S8) [26,27]. This showed its hydrophobic nature. Since it was observed that **1** contained such surface periodic alkyl chain distribution, and as ligand property gets translated into the MOF structure [26,27], we coated it on a glass substrate and proceeded to measure water contact angles. For the experiment, a 4 μl volume of water droplet was placed on different positions and images were recorded to measure the contact angle. The coated surface showed contact angles of 169 ± 1° (figure 2a inset). This proved the superhydrophobicity of the structure. Interestingly, this proves that rigidity and periodicity of surface projected alkyl chains are the necessary criteria for inducing water repellence in a structure. As **H_2OPE-C_{18}** lacks periodicity due to the absence of a rigid framework structure, it did not portray superhydrophobicity. The elongated conjugation present in the structure then, made us to delve into the investigation of the optoelectronic properties of **1**. When dispersed in THF, it showed characteristic two absorption bands at 320 and 380 nm, respectively (supplementary figure S9). Upon excitation at 380 nm, the THF dispersion of **1** gave an emission maximum at 450 nm (figure 2b). Images of the dispersed state under UV light also showed a bright cyan emission (figure 2b inset). In the solid state, **1** absorbed at 400 nm and emitted at 485 nm upon excitation at 400 nm (supplementary figure S10a, b). Images of **1** under UV also revealed bright greenish emission (supplementary figure S10b inset). This emission is linker-based as **H_2OPE-C_{18}** also absorbs and emits in the same region (supplementary figure S11). The measured quantum yield gave a value of 22%. This revealed the excellent optical output of **1**. Fluorescence decay profiles, monitored at 485 nm, upon excitation of **1** at 404 nm, revealed an excited state lifetime of 1.1 ns (supplementary figure S12). To find out the electrochemical band gap, we further carried out cyclic voltammetric measurements on **1** on a GCE in anhydrous acetonitrile with TBAP as the supporting electrolyte (supplementary figure S13). Well-defined oxidation and reduction peaks were obtained from which the band gap

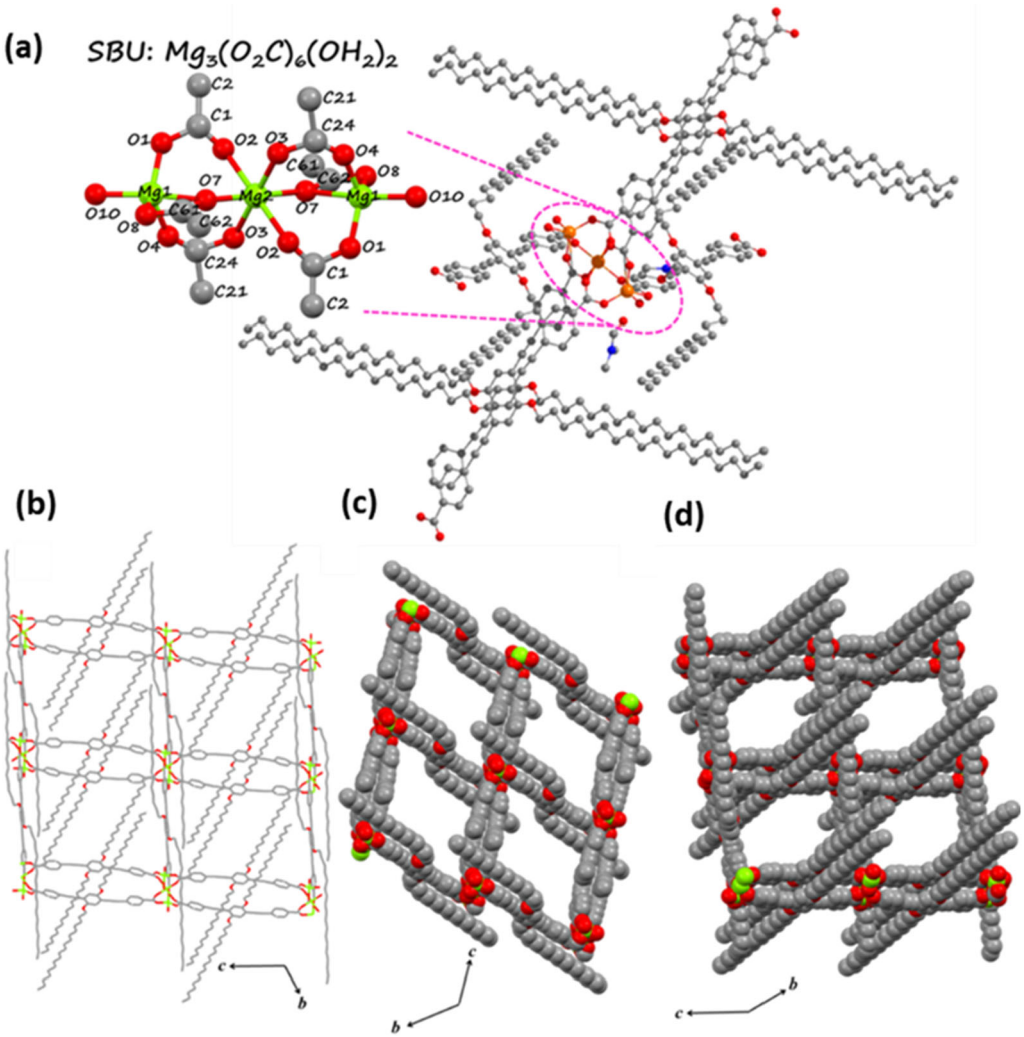

Figure 1. Single crystal structure of **1**: (**a**) asymmetric unit showing the coordination of OPE dicarboxylates around the Mg centres. Inset: representation of the $Mg_3(O_2C)_6(OH_2)_2$ SBU showing the coordination environment around Mg centres. (**b**) View showing the 2D grid formation. (**c**) Spacefill model view of the pores formed in the 2D grid. (**d**) Spacefill model showing the surface projected alkyl chains in the 2D grid. (Solvent molecules have been omitted for clarity.)

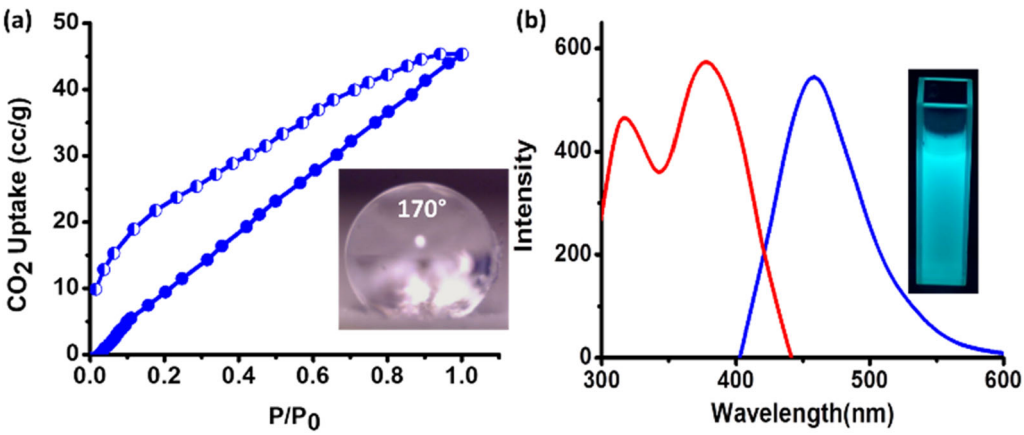

Figure 2. (**a**) CO_2 adsorption isotherm at 195 K for **1**. Inset: water contact angle image on **1** coated glass substrate. (**b**) PL plot of **1** in THF dispersed state. Inset: image of **1** dispersed in THF under UV.

was calculated to be 2.55 eV. We then went on to investigate the electrical conduction property of **1**. As we were able to grow its single crystals as well as create thin films, we decided to experiment on both the forms. Electrical measurements on different faces of the single crystals were carried out using wire-paste approach, while aluminium contacts were used in the thin film approach. A two-probe method was employed to carry out all the measurements in an open atmosphere under ambient conditions. For the single crystal measurements, silver paste was applied to opposite sides of side face and broad face of the single crystals via a bonding machine (figure 3a, c). Further, copper wires were attached to the contacts and *I–V* characteristics were measured using a Keithley 2450 sourcemeter. The obtained conductivities for the side face of the block-shaped crystal was 3.77×10^{-10} S cm^{-1}, while that of the long face of the crystal was measured to be 1.19×10^{-9} S cm^{-1} (figure 3b, d). These values point to an almost isotropic conductivity in different faces of single crystals of **1**. Going back to the structural description, we see that **1** packs in almost similarly in perpendicular directions via OPE dicarboxylate connections to the $Mg_3(O_2C)_6(OH_2)_2$ SBU nodes. The pathway of charge transport therefore occurs via the 2D grid-like conjugated

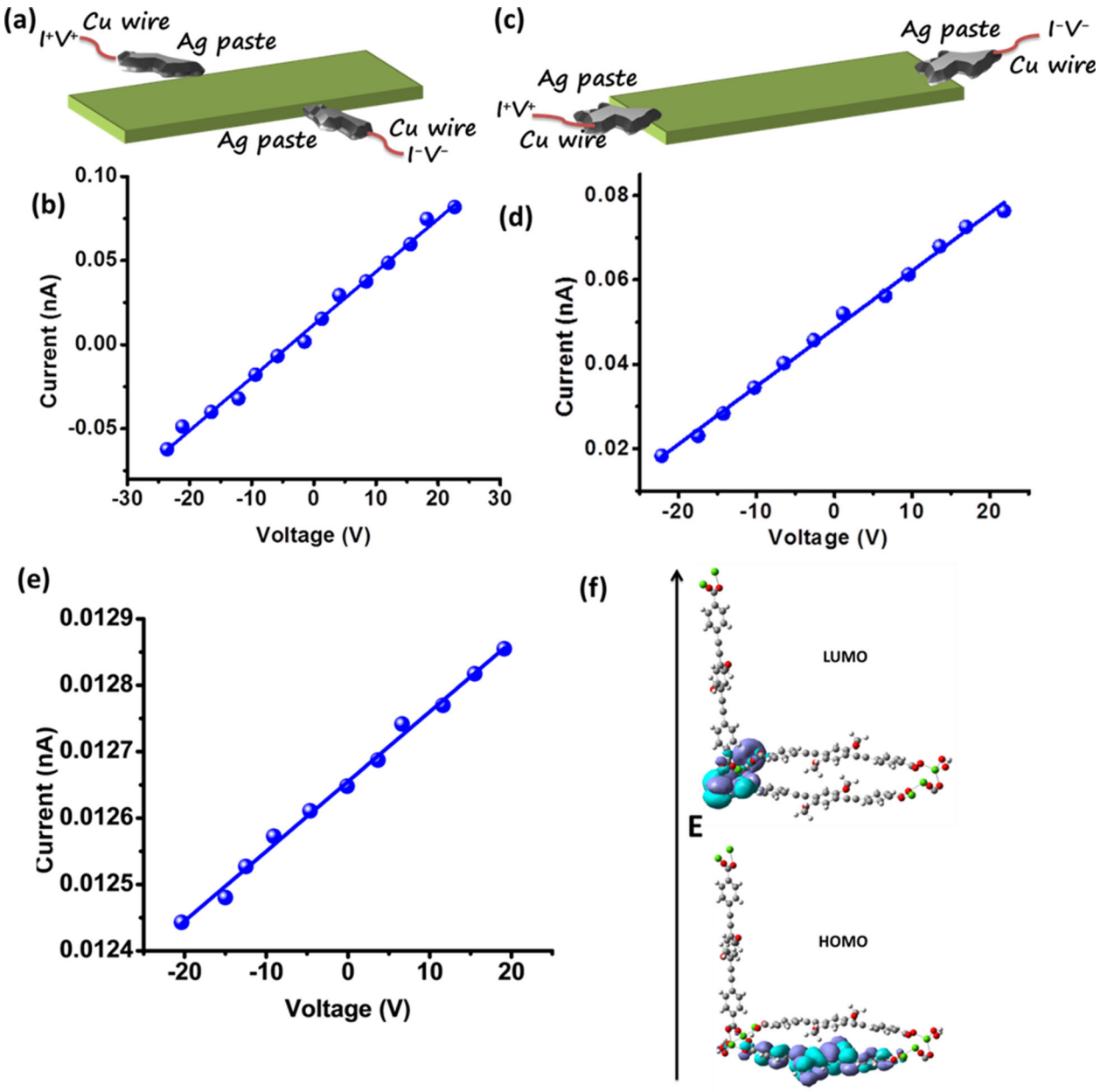

Figure 3. Schematic showing the experimental setup used for measurement of *I–V* characteristics of (**a**) side face, (**c**) broad face of **1** single crystals of **1**. *I–V* plots for (**b**) side face, (**d**) broad face of **1** single crystals, (**e**) thin film of **1** and (**f**) HOMO (lower) and LUMO (upper) plots for **1** shown using a fragmented unit for pictorial clarity.

OPE backbone. This results in comparable conductivities obtained from perpendicular faces of block-shaped single crystals of **1**. Hence, it is apparent that the mode of charge transport is 'through bond' rather than a 'through space' route. To further confirm this hypothesis, we carried out DFT calculations on **1**. The HOMO–LUMO gap for the **1** was found to be 2.23 eV which matches closely to the experimental band gap (figure 3f). Furthermore, HOMO wave functions reside on the OPE molecules of the 1D column, whereas the LUMO mainly resides on the Mg^{II} *p*-orbitals and surrounding chelating atoms of the SBU (figure 3f). This further proves our conjecture that a charge transport occurs via the conjugated bonds and metal atom present throughout the structure. The thin film conductivity of **1** was measured to be 8.82×10^{-10} S cm^{-1} (figure 3e). This is an intermediate value of that obtained from both faces of the single crystal. The reason can be attributed to the isotropic distribution of OPE backbones obtained upon thin film formation which gives a transitional value of conductivity for **1**.

4. Conclusions

To summarize, a Mg^{II}-based MOF with organic π-conjugated linker (**H_2OPE-C_{18}**) having oxy-octadecyl side chains, has been crystallized and structurally well characterized. The permanent porous structure obtained shows a 2D grid-like extension with surface-projected alkyl chains. This further led to superhydrophobicity of the surface of **1**. Owing to the use of the conjugated linker, inherent luminescence in **1** with a high quantum output was also realized. The extended conjugation present in the system also generated facile charge transport in **1**. Electrical measurements on different faces of the single crystals and thin films of **1** revealed its semiconducting property. Finally, the fabrication of a material that has moisture-resistant optoelectronic properties and could have promise in device applications.

Acknowledgements

We thank Dr Saurav Islam for helping in conductivity measurements. SR acknowledges UGC (Govt. of India) and SB acknowledges the INSPIRE program for fellowship. TKM gratefully acknowledges DST, India (project nos. MR-2015/001019 and TRC-DST/C.14.10/16-2724, JNCASR), and JNCASR for funding.

References

[1] Kitagawa S, Kitaura R and Noro S-I 2004 *Angew. Chem. Int. Ed.* **43** 2334
[2] Maji T K, Matsuda R and Kitagawa S 2007 *Nat. Mater.* **6** 142
[3] Li H, Eddaoudi M, O'Keeffe M and Yaghi O M 1999 *Nature* **402** 276
[4] Roy S, Chakraborty A and Maji T K 2014 *Coord. Chem. Rev.* **273–274** 139
[5] He Y, Li B, O'Keeffe M and Chen B 2014 *Chem. Soc. Rev.* **43** 5618
[6] Müller-Buschbaum K, Beuerle F and Feldmann C 2015 *Micropor. Mesopor. Mater.* **216** 171
[7] Zhou H-C and Kitagawa S 2014 *Chem. Soc. Rev.* **43** 5415
[8] Adams R, Carsons C, Ward J, Tannenbaum R and Koros W 2010 *Micropor. Mesopor. Mater.* **131** 13
[9] Heine J and Müller-Buschbaum K 2013 *Chem. Soc. Rev.* **42** 9232
[10] Horcajada P, Chalati T, Serre C, Gillet B, Sebrie C, Baati T *et al* 2010 *Nat. Mater.* **9** 172
[11] Shimizu G K H, Taylor J M and Kim S 2013 *Science* **341** 354
[12] Carné-Sánchez A, Imaz I, Cano-Sarabia M and Maspoch D 2013 *Nat. Chem.* **5** 203
[13] Sun L, Park S S, Sheberla D and Dincă M 2016 *J. Am. Chem. Soc.* **138** 14772
[14] Campbell M G, Liu S F, Swager T M and Dincă M 2015 *J. Am. Chem. Soc.* **137** 13780
[15] Rana S, Rajendra R, Dhara B, Jha P K and Ballav N 2016 *Adv. Mater. Interfaces* **3** 1500738
[16] Sun L, Campbell M G and Dincă M 2016 *Angew. Chem. Int. Ed.* **55** 3566
[17] Sheberla D, Sun L, Blood-Forsythe M A, Er S, Wade C R, Brozek C K *et al* 2014 *J. Am. Chem. Soc.* **136** 8859
[18] Stavil V, Talin A A and Allendorf M D 2014 *Chem. Soc. Rev.* **43** 5994
[19] Talin A A, Centrone A, Ford A C, Foster M E, Stavila V, Haney P *et al* 2014 *Science* **343** 66
[20] Roy S, Das M, Bandyopadhyay A, Pati S K, Ray P P and Maji T K 2017 *J. Phys. Chem. C* **121** 23803
[21] Bhattacharya B, Layek A, Alam Md M, Maity D K, Chakrabarti S, Ray P P *et al* 2014 *Chem. Commun.* **50** 7858
[22] Wu G, Huang J, Zang Y, He J and Xu G 2017 *J. Am. Chem. Soc.* **139** 1360
[23] Surya S G, Nagarkar S S, Ghosh S K, Sonard P and Rao V R 2016 *Sens. Actuators B Chem.* **223** 114
[24] Cui Y, Yue Y, Qian G and Chen B 2012 *Chem. Rev.* **112** 1126
[25] Rocha J, Carlos L D, Paz F A A and Ananias D 2011 *Chem. Soc. Rev.* **40** 926
[26] Roy S, Suresh V M and Maji T K 2016 *Chem. Sci.* **7** 2251
[27] Roy S, Suresh V M, Hazra A, Bandyopadhyay A, Laha S, Pati S K *et al* 2018 *Inorg. Chem.* **57** 8693
[28] Suresh V M, George S J and Maji T K 2013 *Adv. Funct. Mater.* **23** 5585
[29] Suresh V M, Chatterjee S, Modak R, Tiwari V, Patel A, Kundu T K *et al* 2014 *J. Phys. Chem. C* **118** 12241
[30] Samanta D, Verma P, Roy S and Maji T K 2018 *ACS Appl. Mater. Interfaces* **10** 23140
[31] Samanta D, Roy S, Sasmal R, Das Saha N, Viswanatha R, Agasti S S *et al* 2019 *Angew. Chem. Int. Ed.* **58** 5008
[32] Roy S, Hazra A, Bandyopadhyay A, Raut D, Madhuri P L, Shankar Rao D S *et al* 2016 *J. Phys. Chem. Lett.* **7** 4086
[33] Bhattacharyya S, Sobczak S, Półrolniczak A, Roy S, Samanta D, Katrusiak A *et al* 2019 *Chem. Eur. J.* **25** 6092
[34] Nguyen J G and Cohen S M 2010 *J. Am. Chem. Soc.* **132** 4560

[35] Rao K P, Higuchi M, Sumida K, Furukawa S, Duan J and Kitagawa S 2014 *Angew. Chem. Int. Ed.* **53** 8225
[36] Chen T-H, Popov I, Zenasni O, Daugulis O and Miljanic O S 2013 *Chem. Commun*. **49** 6846
[37] Serre C 2012 *Angew. Chem. Int. Ed.* **51** 6048
[38] Tan T T Y, Reithofer M R, Chen E Y, Menon A G, Hor T S A, Xu J *et al* 2013 *J. Am. Chem. Soc*. **135** 16272